Nuclear Instruments and Methods in Physics Research A258 (1987) 58–66
North-Holland, Amsterdam

DETERMINATION OF TRACE ELEMENTS IN BGO BY NEUTRON ACTIVATION ANALYSIS

T.Q. ZHOU, H.R. TAN and C.F. HE
Shanghai Institute of Ceramics, Shanghai, China

R.Y. ZHU and H.B. NEWMAN *
California Institute of Technology, Pasadena, CA 91125, USA

Received 20 February 1987

We report on the determination of trace elements in a set of $Bi_4Ge_3O_{12}$ (BGO) crystals by neutron activation analysis. By using doped polycrystalline BGO powders as calibration standards, we have measured the concentrations of Al, Mn, Cu, Co, Cr and Fe in the crystals with a sensitivity of 0.5–500 ppb, and we have determined the segregation coefficients. We have also studied the correlation between the trace elements and the "radiation damage" (color center formation) effect

1. Introduction

Bismuth germanate ($Bi_4Ge_3O_{12}$) is coming into increasing use for electromagnetic calorimetry in high energy physics experiments [1]. In addition to having high mechanical strength, and being nonhygroscopic, BGO has the advantages of high stopping power, large enough scintillation efficiency to use Si photodiode readout above a few MeV, and very good energy resolution [2].

One of the properties which might limit the use of BGO for high precision calorimetry is its sensitivity to "radiation damage". Following exposure to ionizing radiation, BGO exhibits changes in light transmission due to the formation of color centers. Its emission spectrum may also be altered, but measurements [3] to date indicate that this may be a minor effect.

Starting in 1984, we began a program of research which focused on the study of the underlying mechanism responsible for radiation damage in BGO. A practical goal of this program is to find a method which can be applied during the crystal production process to increase the crystals' radiation hardness. This paper presents results of part of the study, in which we determined the concentration of trace elements in a series of specially prepared doped and undoped crystals. We correlated the concentration and type of dopant with the susceptibility to radiation damage.

We chose neutron activation analysis (NAA) as the preferred method of analysis in this study, because the standard spectrometric methods ** require samples in the form of a chemical solution. The poor solubility of BGO in all common reagents makes these analyses difficult, and limits the sensitivity and accuracy of the standard methods. NAA also has the advantage that one need only be concerned with surface contaminants which are easily removed by washing the solid samples just prior to activation.

The use of NAA allowed us to search for several trace elements in a short series of runs. We measured Al, Mn, Co, Cr, and Fe which previous studies [3] had indicated were likely to be the source of the radiation damage effect. The run parameters were set by compromising between maximum sensitivity [5] and short overall run time.

Sects. 2 and 3 of this report describe the experimental conditions and procedures used for the measurements. Sect. 4 focuses on the data analysis, and sect. 5 presents the results and conclusions.

2. Experimental conditions

2.1. Crystal samples

Most of the crystal samples were grown with the Bridgeman–Stockbarger method at the Institute of

* Supported in part by US Department of Energy Contract no. DE-AC03-81-ER40550

** These include flame atomic absorption spectrometry (FAAS), flame atomic emission spectrometry (FAES), and inductively coupled and direct coupled plasma atomic emission spectrometry (ICPAES and DCPES) [4].

Table 1
Samples and dopant concentrations in melt

Sample	Weight [g]	Concentration [ppm]	Dimensions [cm]
Al-doped	21.0	5.4	1×1×3
Mg-	21.1	5.1	1×1×3
Cu-	21.2	12.7	1×1×3
Ni-	20.7	11.7	1×1×3
Si-	21.0	5.3	1×1×3
Mn-	20.9	11.0	1×1×3
Ga-	20.5	13.2	1×1×3
Fe1-	17.4	5.6	0.9×0.9×3
Fe2-	17.4	11.2	0.9×0.9×3
Fe3-	16.2	16.7	0.9×0.9×3
Fe4-	16.7	22.3	0.9×0.9×3
Ge1-	21.1	145	1×1×3
Ge2-	21.5	1451	1×1×3
Bi1-	21.0	418	1×1×3
Bi2-	21.0	4200	1×1×3
Ca-	15.0	8.4	1×1×2.2
Cr-	20.7	10.4	1×1×3
Co-	21.3	11.8	1×1×3
Pb1-	20.4	20.7	1×1×3
Pb2-	21.1	41.4	1×1×3
Pb3-	20.9	62.2	1×1×3
Pb4-	20.8	82.9	1×1×3
L-1	20.9	undoped	1×1×3
L-3	13.8	undoped	1×1×2
O-5	13.5	undoped	1×1×2
M2	13.6	Harshaw	1×1×2
Hs	27.8	Harshaw	1×1×3.9

Ceramics in Shanghai, China. Two of the crystal samples were grown by the Harshaw–Filtrol Co [6]. A large Shanghai crystal was grown from a melt of 5N Bi_2O_3 and 6N GeO_2 powders, mixed in the stoichiometric ratio 2 : 3. The crystallization was repeated three times for purification.

Using this crystal as raw material, different dopants

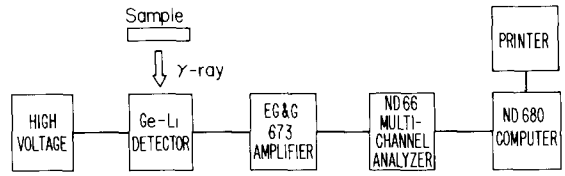

Fig. 1. Instrumental setup of neutron activation measurement.

which could conceivably contaminate the crystals (inherent from raw materials or introduced during the production process) were added to the crystal melt. The dopant level in the melt was of the order of 0.2 mmol/(kg BGO), which corresponds to 5–50 ppm by weight, as summarized in table 1. For dopants Fe and Pb, samples were prepared at several different dopant levels.

All the crystal samples were cleaned by immersing the crystals in an HNO_3 solution for 3 hours, by immersing them in acetone for another 3 hours, and then washing them in pure water.

2.2. Calibration sample

We made the calibration samples by mixing polycrystalline BGO powder from the Johnson–Matthey Co. [7] with different amounts of weights of target impurity oxides. We were not concerned by the fact that the powder samples came from raw materials mined in the Western Hemisphere while some of the raw materials used in the crystal samples originated in China. The isotopic abundances in materials are known to depend little on the site of origin, especially for heavy elements [8].

We used a rectangular cell to contain the powder samples, so that the geometrical and self-absorption corrections were the same for the powder and the crystal samples. The use of BGO powder as a calibra-

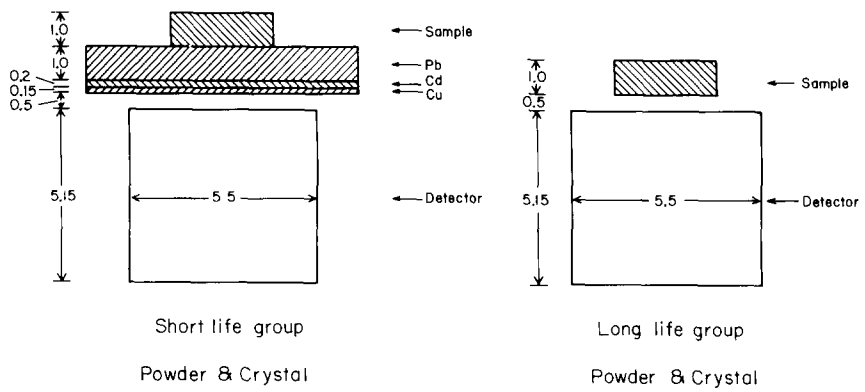

Fig. 2. Geometrical arrangement for the measurements.

tion standard also had the advantage of giving the same series of γ-ray background lines as that which resulted from irradiating the crystals. This background comes mainly from the activation of ^{77}Ge, and results in a large number of γ-ray lines with half-lives ranging up to a maximum of 11.3 h.

As a cross-check, we also used a National Bureau of Standards calibration sample, type NBS 1571 [9], which contains a known amount of all the target impurities except Cu. The results obtained from the NBS sample were compared to the known trace levels to help determine the systematic errors in our runs.

2.3. Reactor

The Triga Mark I reactor at the University of California at Irvine was used in this measurement. It has a maximum thermal neutron flux of $(2.00 \pm 0.04) \times$

Table 2
Characteristics of target elements

	Al	Mn	Cu	Cr	Co	Fe
Isotope	^{27}Al	^{55}Mn	^{65}Cu	^{50}Cr	^{59}Co	^{58}Fe
σ [a] [b]	0.233	13.3	2.17	15 8	20.20	1.16
Abundance [%]	100	100	30.8	4.35	100	0.3
E [keV]	1779	1810	1039	320	1173	1099
DBR [b] [%]	100	30	9	9.8	99.9	56
Half-life	2.24 min	2.58 h	5.1 min	27.7 d	5 27 yr	44.6 d

[a] σ is the thermal-neutron capture cross section.
[b] DBR is the decay branching ratio.

Table 3
Calculated and measured sensitivity

Element	Φ [n/cm^2 s]	Shielding	T_A	T_W	T_C	S [a] [ppb]	S_m [b] [ppb]
Al	0.64×10^{12}	1.5 cm Pb	1 min	2 min	5 min	26	30
Cu	0.64×10^{12}	1.5 cm Pb	1 min	2 min	5 min	460	500
Mn	0.64×10^{12}	1.5 cm Pb	1 min	2 min	5 min	52	31
Cr	2.0×10^{12}	No	5 h	15 d	4 h	1 9	29
Co	2.0×10^{12}	No	5 h	15 d	4 h	0.5	0.3
Fe	2.0×10^{12}	No	5 h	15 d	4 h	130	110

[a] S is calculated sensitivity [5].
[b] S_m is measured sensitivity from this work.

Table 4
Powder standards calibration data

Sample	Al	Mn	Cu	Cr	Co
Φ [n/cm^2 s]	0.064×10^{12}	0.064×10^{12}	0.064×10^{12}	2×10^{12}	2×10^{12}
T_A	1 min	1 min	1 min	5 h	5 h
T_W	2 min	2 min	2 min	643.5 h	643.5 h
T_C	5 min	5 min	5 min	24 min	24 min
Shielding	PCC [a]	PCC [a]	PCC [a]	No	No
Counts_{STD1}	876 ±32	223 ±17	102 ±22	5068±106	28713±179
Weight [μg]	82 ± 3	54 ± 4	106 ± 3	48± 4	57± 5
Counts_{STD2}	1159 ±37	449 ±23	145 ±26	14142±176	49370±235
Weight [μg]	119 ± 2	107 ± 3	139 ± 5	132± 3	107± 3
Counts_{STD3}	2088 ±49	733 ±29	272 ±34	14677±188	78331±296
Weight [μg]	197 ± 3	162 ± 4	214 ± 3	157± 4	162± 3
Counts_{STD4}	2259 ±52	980 ±34	479 ±34	19452±213	103251±349
Weight [μg]	235 ± 2	247 ± 3	424 ± 3	210± 3	215± 3
Counts/μg	9.6± 0.2	4.0± 0.1	1.1± 0.2	90± 2	480± 8

[a] PCC: 1.0 cm Pb, 0.2 cm Cd and 0.15 cm Cu were placed between sample and detector

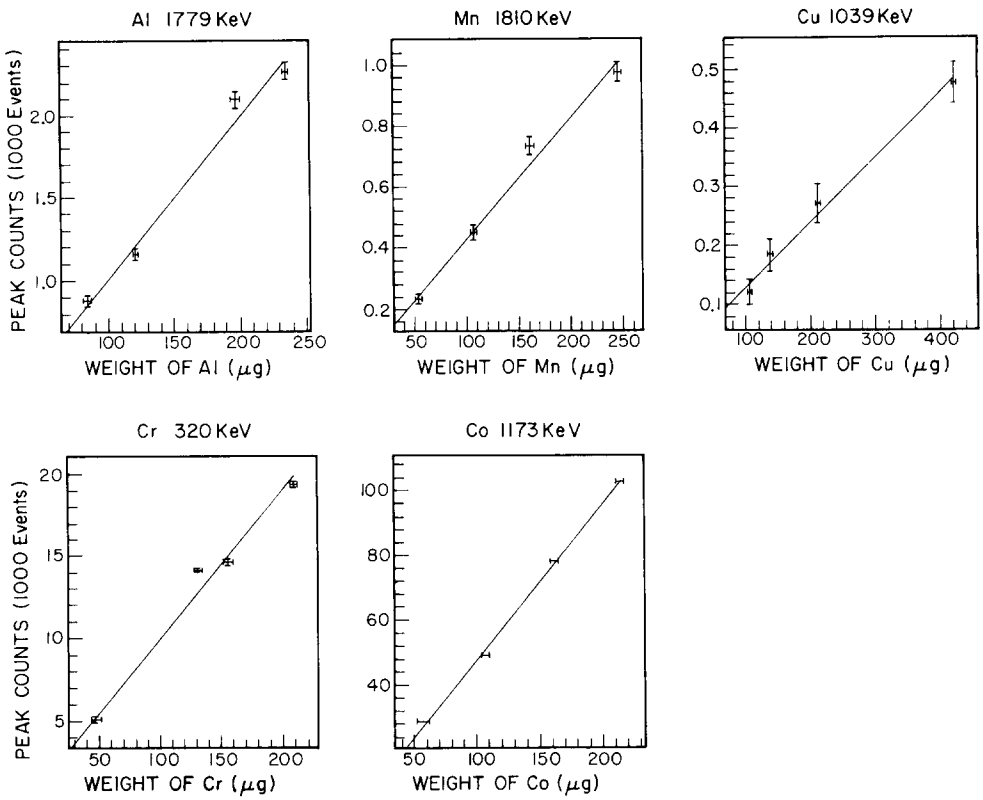

Fig. 3. Dependence of γ-ray peak counts on trace weight for different traces.

Table 5a
Short lifetime group data. The experimental conditions are $\Phi = 0.64 \times 10^{12}$ n/cm^2 s, $T_A = 1$ min, $T_W = 2$ min, $T_C = 5$ min and $G = 1.5$ cm Pb, 0.2 cm Cd and 0.15 cm Cu.

Sample	Al (1779 keV)	Mn (1810 keV)	Cu (1039 keV)
Al	560±31	8±12	168±53
Mg	245±26	0±14	67±54
Cu	735±35	7±13	92±54
Ni	156±21	0±13	58±52
Si	1577±48	14±14	83±54
Mn	90±21	185±20	187±52
Ga	75±20	0±13	105±52
Fe1	156±22	2±12	159±50
Fe2	102±21	15±13	189±50
Fe3	111±19	6±12	102±48
Fe4	133±21	0±11	100±50
Ge1	101±20	3±13	151±52
Ge2	1954±52	0±13	197±55
Bi1	244±25	25±14	18±54
Bi2	1997±53	0±13	144±53
Ca	64±19	0±11	173±47
Cr	248±24	0±13	64±53
Co	1546±47	16±13	95±55
Pb1	104±20	0±14	124±53
Pb2	90±20	0±13	161±53
Pb3	239±25	6±13	81±52
Pb4	204±24	0±14	128±53
L-1	4213±74	0±15	195±57
L-3	190±22	12±11	152±44
O-5	150±21	0± 8	62±45
M2	246±19	4±10	82±46

10^{12} n/cm^2 s [10]. A pneumatic system is used to transport the samples between the reactor and the counting station to reduce the waiting time for short lifetime trace measurements.

2.4. Instruments

All the measurements were made with a multichannel analyzer, type ND 66, equipped with an ND 680 computer system. Fig. 1 is a schematic of the setup. The maximum counting rate of the system for accurate measurements is limited by pileup effects to 10 kHz. A 5.15 cm thick 5.5 cm diameter Ge(Li) semiconductor detector with a resolution of 2.45 keV (fwhm) was used. A 4 inch thick iron can shielded the detector from low energy room background.

For the short lifetime element measurements, a Pb plate shield was placed between the sample and the detector to reduce the low energy background from the Compton scattering of ^{77}Ge peaks. A Cd plate was used to remove the resultant Pb X-rays, and a Cu plate then removed the secondary Cd X-rays. Fig. 2 shows the geometrical arrangement used for the measurements. All dimensions shown are in cm.

Table 5b
Long lifetime group data. The experimental conditions are $\Phi = 2\times10^{12}$ n/cm^2 s, $T_A = 5$ h and without shielding materials

Sample	Cr (320 keV)	Co (1173 keV)	Fe (1099 keV)	T_W [h]	T_C [min]
Al-doped	0± 417	0±21	0±20	422.8	240
Mg-	0± 413	9±21	33±20	427.0	240
Cu-	0± 316	41±24	9±25	525.6	240
Ni-	510± 421	162±22	9±21	545.0	240
Si-	0± 422	48±22	38±21	407 7	240
Mn-	0± 786	60±35	94±31	384.5	720
Ga-	0± 401	0±20	2±20	431.1	240
Fe1-	0± 605	144±32	82±26	435.5	600
Fe2-	0± 639	26±31	128±28	412.5	600
Fe3-	0± 421	123±34	152±29	553.5	600
Fe4-	0± 447	83±34	176±30	531.5	600
Ge1-	0± 333	43±20	33±19	495.1	240
Ge2-	0± 334	48±20	17±20	499.2	240
Bi1-	0± 354	10±21	26±21	503.4	240
Bi2-	0± 321	7±21	10±21	519.0	240
Ca-	2±2250	0±21	21±21	594 0	240
Cr-	3034± 409	26±22	14±21	549.1	240
Co-	0± 222	5853±83	0±37	645.2	240
Pb1-	0± 436	27±21	13±21	399.2	240
Pb2-	0± 438	19±20	18±20	403.6	240
Pb3-	0± 269	31±21	23±20	566.4	240
Pb4-	0± 275	48±21	23±21	570.7	240
L-1	0± 521	0±32	23±27	507.7	600
L-3	0± 231	14±21	5±20	574 9	240
O-5	0± 203	27±21	0±19	618.8	240
M2	0± 353	81±32	16±25	579.2	600
HS	0± 282	0±21	12±22	589.9	240

3. Experimental procedure

The sensitivity of neutron activation analysis depends on the thermal neutron capture cross section, the natural abundance of the target isotope, and the lifetime of the excited states which lead to the measured γ-rays. The sensitivity also depends on the running conditions, including the neutron flux, activation time, the time between the end of activation and the measurement, the γ-ray counting time and the amount of shielding material between the activated sample and the detector. The resultant lower limit of sensitivity for Al, Mn, Cu, Co, Cr and Fe is of order 10^{-5} to 1 μg [11]. In our case, the large number of lines resulting from activation of ^{77}Ge in BGO, and significant self-absorption in the sample limited the overall sensitivity.

Using techniques developed by Zhu [5], we calculated the optimized experimental conditions for determinations of various trace elements in BGO. The experimental conditions used in this measurement were a compromise between the optimized conditions and the cost of reactor and detection time. Table 3 lists the running parameters and corresponding calculated sensitivities.

The target trace elements were divided into two groups according to their decay lifetimes. The short

Table 6
Correction factors

Element	Al (1779 keV)	Mn (1810 keV)	Cu (1039 keV)	Cr (320 keV)	Co (1173 keV)
$\mu_{crystal}$ [cm^{-1}]	0.35	0.35	0.48	2.1	0.45
μ_{powder} [cm^{-1}]	0.175	0.175	0.24	1.05	0.225
C_Φ	0.1	0.1	0.1	1.0	1.0
C_G	1	1	1	1	1
C_{A1}	1	1	1	1	1
C_{A2}	1.09	1.09	1.12	1.48	1.11

lifetime group included Al, Mn and Cu. The long lifetime group included Cr, Co and Fe. Table 2 lists the thermal neutron capture cross section, the natural abundance, the γ-ray peak energy, the decay branching ratio of the isotopes and the half-life of all target trace elements.

We define the following five parameters to describe the experimental procedure:

Φ : the neutron flux used;
T_A : the neutron activation time;
T_W : the waiting time before the start of the γ-ray counting;
T_C : the γ-ray counting time;
G : the geometrical arrangement of the sample, and the shielding materials between the sample and the Ge(Li) detector.

The total peak counts were taken by integrating the γ-ray spectrum over the range of twice the fwhm around each target peak position. The background counts were taken in sidebands on either side of the peak.

Table 4 shows the experimental conditions and the detailed counting results obtained with the calibration standards. A least-squares fit was used to obtain the calibration constants in units of counts/(μg of target element). Fig. 3 shows the fit results obtained from the analysis of γ-ray peaks of Al, Mn, Cu, Cr and Co.

The experimental parameters and counting results for the BGO sample measurements are listed separately in tables 5a and 5b for the short and long lifetime trace element measurements.

4. Data analysis

The total γ-ray counts, N_S, in the Ge(Li) detector for a specific target trace element can be written as [11]:

$$N_S = N\sigma\Phi F_G F_{A1} F_{A2} F_T, \quad (1)$$

where N is the number of target trace element atoms, Φ is the flux of thermal neutrons, in units of n/cm^2 s, σ is the thermal neutron capture cross section, in units of cm^2, F_G is the geometrical acceptance and efficiency of the detector, F_{A1} is the absorption factor due to the shielding material, F_{A2} is the self-absorption factor of the sample, and F_T is the time factor, in units of s, which expresses the time dependence of the counting rate on the activation, waiting and counting time:

$$F_T = \tau(1 - e^{-T_A/\tau})\, e^{-T_W/\tau}(1 - e^{-T_C/\tau}). \quad (2)$$

In eq. (2) T_A, T_W, T_C are defined as in sect. 3 and τ is the lifetime of the isotope.

Table 7
Measured trace concentrations

Sample	Al [ppm]	Mn [ppm]	Cu [ppm]	Cr [ppm]	Co [ppb]	Fe [ppm]
Al-doped	0.30 ± 0.02	< 0.031	0.81 ± 0.26	< 0.052	< 0.5	< 0.13
Mg-	0.13 ± 0.01	< 0.036	< 0.52	< 0.052	< 0 5	< 0.13
Cu-	0.39 ± 0.02	< 0.033	< 0.52	< 0.043	< 0.5	< 0.17
Ni-	0.09 ± 0.01	< 0.034	< 0.51	< 0.060	0.7 ± 0.2	< 0.15
Si-	0.85 ± 0.03	< 0.036	< 0 52	< 0 052	0.5 ± 0.2	< 0.13
Mn-	0 05 ± 0.01	0.241 ± 0.026	0 91 ± 0.25	< 0.032	< 0.3	< 0.13
Ga-	0 04 ± 0.01	< 0.035	0 52 ± 0.26	< 0.052	< 0.5	< 0.13
Fe1-	0.10 ± 0.01	< 0.038	0.93 ± 0.29	< 0.037	0 8 ± 0 2	0.13 ± 0.04
Fe2-	0.07 ± 0.01	< 0.041	1.10 ± 0.29	< 0.038	< 0 3	0.20 ± 0.04
Fe3-	0.08 ± 0.01	< 0.040	0 64 ± 0.30	< 0.032	0.7 ± 0.2	0 27 ± 0.05
Fe4-	0.09 ± 0.01	< 0.036	< 0 61	< 0.032	0.5 ± 0.2	0.30 ± 0.05
Ge1-	0.05 ± 0.01	< 0.034	0 73 ± 0.25	< 0.044	0.5 ± 0.2	< 0.13
Ge2-	1 03 ± 0.03	< 0.033	0.93 ± 0.26	< 0.044	0.5 ± 0.2	< 0.13
Bi1-	0.13 ± 0 01	< 0.036	< 0.52	< 0.048	< 0.5	< 0.14
Bi2-	1.08 ± 0.03	< 0.034	0.7 ± 0.26	< 0.044	< 0.5	< 0.14
Ca-	0.05 ± 0.01	< 0.040	1.17 ± 0.32	< 0.067	< 0.6	< 0.21
Cr-	0.14 ± 0.01	< 0.034	< 0.52	0.219 ± 0.030	< 0.5	< 0.15
Co-	0.82 ± 0.03	< 0.033	< 0.52	< 0.050	63.7 ± 0.9	< 0.27
Pb1-	0.06 ± 0.01	< 0.037	0.62 ± 0.27	< 0.055	< 0.5	< 0.14
Pb2-	0.05 ± 0.01	< 0.034	0.78 ± 0.26	< 0.053	< 0.4	< 0.13
Pb3-	0.13 ± 0.01	< 0.034	< 0.51	< 0.039	< 0.5	< 0.14
Pb4-	0.11 ± 0.01	< 0.037	0 63 ± 0.26	< 0.040	0.5 ± 0.2	< 0.15
L-1	2.29 ± 0.04	< 0.039	0 95 ± 0 28	< 0.029	0.3	< 0.07
L-3	0.16 ± 0.02	< 0.043	1.12 ± 0.32	< 0.051	< 0.7	< 0.21
O-5	0.13 ± 0.02	< 0.032	< 0.68	< 0.048	< 0.7	< 0.21
M2	0.20 ± 0.02	< 0.040	< 0.69	< 0.032	0.6 ± 0.2	< 0 11
HS	–	–	–	< 0.032	< 0.4	< 0.12

By using the calibration constants obtained in sect. 3, the concentration of trace elements in the sample S, in units of ppm, can be written as:

$$S = \frac{\text{weight of trace elements } (\mu g)}{\text{weight of sample (g)}} = \frac{1}{W_S}\frac{N_S}{C}\frac{\Phi_C F_{GC} F_{A1C} F_{A2C} F_{TC}}{\Phi_S F_{GS} F_{A1S} F_{A2S} F_{TS}}, \quad (3)$$

where W_S is the weight of the sample, in units of g, C is the calibration constant in units of counts/μg, the subscript C refers to the calibration run, and the subscript S refers to the sample run.

We then define the correction factors as follows:

$$C_X = \frac{X_C}{X_S}; \quad (4)$$

where X can be Φ, F_G, F_{A1}, F_{A2} and F_T.

By using eq. (4), eq. (3) can be written as:

$$S = \frac{1}{W_S}\frac{N_S}{C} C_\Phi C_G C_{A1} C_{A2} C_T. \quad (5)$$

The determination of the correction factors C_Φ and C_T is straightforward. The correction factors C_G and C_{A1} are unity, since exactly the same geometry is used in both calibration and sample runs.

The self-absorption factor C_{A2}, due to the difference in the photon mass attenuation factors between the crystal and the polycrystalline powder, can be approximated as:

$$C_{A2} = \frac{\mu_{cryst} D_{cryst}}{\mu_{powder} D_{powder}} \frac{1 - e^{-\mu_{powder} D_{powder}}}{1 - e^{-\mu_{cryst} D_{cryst}}}, \quad (6)$$

where μ is the photon mass attenuation coefficient, D is the thickness of the sample, and the subscripts cryst and powder refer to the crystal and powder standard respectively. Table 6 lists the the correction factors for the target elements.

By using the calibration constants in table 4 and the correction factors in table 6, the trace element concentrations were calculated according to eq. (5). The results are listed in table 7.

The errors quoted in table 7 are statistical only. When the counts in the peak were less than 2 standard deviations above the background, we calculated the 95% confidence level lower limit of detection (LLD), as shown in the table.

5. Results and discussion

5.1. Systematic error

As a systematic check, a sample, National Bureau Standard 1571 (NBS 1571), was measured. Table 8 lists the experimental conditions, the correction factors and the results obtained. The nominal trace element levels of NBS 1571 are listed in the last line of table 8, and can be compared to the measured trace element concentrations in NBS 1571 obtained by using the calibrations from our polycrystalline powder. The overall consistency is quite good with the exception of the Cr sample, where the measured concentration was a factor 2 too high. A possible cause for this deviation is the approximations involved in the determination of the correction factors. Our overall estimate of the systematic error in our results, based on these cross-comparisons between the NBS standard and our own powder calibration standards, is 20%.

Table 8
NBS 1571 sample data

Sample	Al	Mn	Cr	Co	Fe
Φ [n/cm^2 s]	0.64 ± 10^{12}	0.64×10^{12}	2×10^{12}	2×10^{12}	2×10^{12}
T_A	1 min	1 min	5 h	5 h	5 h
T_W	2 min	2 min	383.5 h	383.5 h	383.5 h
T_C	5 min	5 min	60 min	60 min	60 min
Shielding	BPCC [a]	BPCC [a]	No	No	No
Counts	2396 ± 52	234 ± 17	264 ± 41	52 ± 17	156 ± 17
C_Φ	0.1	0.1	1.0	1.0	1 0
C_G	1.25	1.25	0.84	0.84	0.84
C_{A1}	1.19	1.19	1.0	1.0	1.0
C_{A2}	0.917	0.917	0.617	0.893	0.893
C_T	1.0	1.0	0.305	0.398	0.338
C_M [b] [ppm]	375 ± 8	88 ± 7	4.7 ± 0.8	0.36 ± 0.10	–
C_S [c] [ppm]	310 ± 100	89 ± 5	2.48 ± 0.34	0.17 ± 0.09	280 ± 50

[a] BPCC: $1 \times 1 \times 3$ cm^3 BGO powder, 1 cm Pb, 0.2 cm Cu were placed between the sample and detector.
[b] C_M is the measured trace level in the NBS 1571 sample.
[c] C_S is the nominal trace level in NBS 1571 [9].

Table 9
Segregation coefficients

	Al	Cu	Mn	Cr	Fe	Co
C_{melt} (ppm)	> 5.4	> 12.7	11.0	10.4	5.6	11.8
$\bar{C}_{cryst}$ (ppm)	0.30	< 0.52	0.24	0.22	0.13	0.064
$\bar{k}$	< 0.056	< 0.04	0.022	0.021	0.023	0.005

5.2. Sensitivity

The results in table 7 show that the trace elements Al, Mn, Cu, Cr, Co and Fe in BGO are determined down to the level of 0.5–500 ppb by use of neutron activation analysis.

The experimental sensitivities obtained can be compared to our predictions in table 3. The overall consistency is quite good for most elements except Cr. While the predicted sensitivity for Cr is 2 ppb, the measured sensitivity is 30 ppb. This discrepancy can be explained by the high background for low energy 320 keV γ-rays from Cr, which was not fully taken into account in our calculations.

5.3. Segregation coefficient

The concentration of different impurities in a finished crystal may be different, even if the same quantity of each dopant is introduced into the crystal melt during the growing process. This is because the distribution of dopant ions between the solid and liquid phase is a complicated process which depends on the growth conditions as well as on the nature of the ionic species [12]. In our case, the mean segregation coefficient, $\bar{k}$, defined as the ratio of the mean concentration in the bulk crystal, $\bar{C}_{cryst}$, to the initial concentration of dopant in the melt, C_{melt}, is simply used to describe the ability of an impurity to enter the solid phase:

$$\bar{k} = \bar{C}_{cryst}/C_{melt}. \quad (7)$$

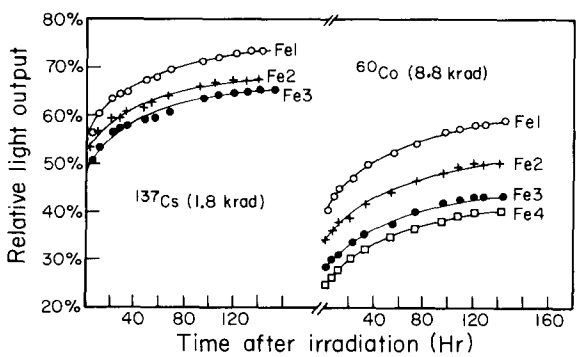

Fig. 4. Recovery curves for light output from irradiated Fe-doped crystals.

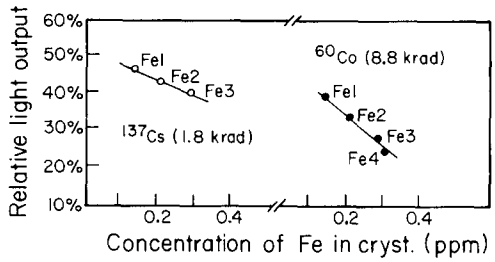

Fig. 5. Relative light output vs concentration of Fe.

Table 9 lists the segregation coefficients of elements Al, Fe, Cr, Co, Cu and Mn. The segregation coefficients of Fe, Cr and Mn are about 0.02, and the segregation coefficient of Fe is 30 times smaller than Barnes' result [13] for BGO crystals synthesized by the Czochralski method.

5.4. Radiation damage

The presence of impurities in BGO crystals affects the properties of the crystals, especially the radiation resistance [14]. A contamination of 200 ppb by weight of some impurities, such as Pb, Fe and Mn, causes serious radiation damage. The detailed quantitative correlation between impurities in BGO and radiation resistance can be found in ref. [15].

Fig. 4 shows the recovery curves for samples doped with different concentrations of Fe from radiation damage induced by exposure to 1.78 krad and 8.8 krad from a ^{137}Cs source and a ^{60}Co source, respectively. The correlation between the degree of radiation damage and the dopant concentration is shown in fig. 5, where the light output (normalized to the pre-irradiation value) of the samples, one hour after irradiation is plotted against the dopant concentration as determined in this work.

Acknowledgements

The authors would like to thank Prof. G. Miller for his help in measurements at UCI and Jingying Lia, Quanshun Shen and Peifa Shao for their help in the preparation of crystal samples. Many helpful discussions with H. Stone are gratefully acknowledged.

References

[1] L3 Collaboration, Technical Proposal (1983); CELLO Collaboration, DESY-CELLO-83-01 (1983); ARGUS Collaboration, DESY report PRC.83/06 (1983).
[2] J.A. Bakken et al. (L3 Collaboration), CERN-EP/86-152 (Oct 1986); J. Iwahori et al., KEK preprint 85-51 (Oct 1985), K. Borer et al., Helv Phys. Acta 57 (1984) 292; H. Dietl et al., Nucl. Instr. and Meth. 235, (1985) 464; L. Adiels et al., Nucl. Instr. and Meth. 244 (1986) 380.
[3] C. Lavıron and P. Lecoq, Nucl. Instr. and Meth. 22 (1984) 45; C. Bieler et al. Nucl. Instr. and Meth. 234 (1985) 435; G.J. Bobbink et al., Nucl. Instr. and Meth. 227 (1984) 470; M. Kobayashi et al., Nucl. Instr. and Meth. 206 (1983) 107; T.Q. Zhou et al, L3 Internal Report (Nov. 1984).
[4] Caltech L3 Group, L3 Internal Report 231 (March 1984).
[5] R.Y. Zhu et al., L3 Internal Report 286 (Apr. 1984).
[6] Harshaw/Filtrol Partnership, 6801 Cochran Rd., Solon, Ohio 44139, USA.
[7] Johnson–Matthey Chemical Co, Orchard Rd., Royston, Hertfordshire SG8 5HE, England.
[8] J. Hoefs, Stable Isotope Geochemistry (New York, 1980).
[9] E.S. Gladney, Informal Report to the National Bureau of Standards, La-8438-MS (1980).
[10] G Miller, Instructions for the Triga Reactor, Univ. of California at Irvine (1973).
[11] V.P. Guinn and J. Hoste, Elemental Analysis of Biological Materials, ed., R.M. Parr (IAEA, Vienna, 1980).
[12] F. Rosenberger, Fundamentals of Crystal Growth, vol. 1 (Springer, New York, 1979).
[13] R. Barnes, J. Cryst. Growth 69 (1984) 248.
[14] C. He et al., Progress Cryst. Growth Charact. 11 (1985) 253
[15] T.Q Zhou et al., CALTECH CALT-68-1392.